Silica films with a single-crystalline mesoporous structure

HIROKATSU MIYATA[1]*, TAKASHI SUZUKI[2], AYUMU FUKUOKA[2], TAKESHI SAWADA[2], MASATOSHI WATANABE[1], TAKASHI NOMA[1], KAZUHIRO TAKADA,[1] TAIHEI MUKAIDE[1] AND KAZUYUKI KURODA[2,3,4]

[1]Leading-Edge Technology Development Headquarters, Canon Inc. 5-1 Morinosato-Wakamiya, Atsugi-shi, Kanagawa 243-0193, Japan
[2]Department of Applied Chemistry, Waseda University, 3-4-1 Ohkubo, Shinjuku-ku, Tokyo 169-8555, Japan
[3]Kagami Memorial Laboratory for Materials Science and Technology, Waseda University, 2-8-26 Nishiwaseda, Shinjuku-ku, Tokyo 169-0051 Japan
[4]CREST, Japan Science and Technology Agency, Japan
*e-mail: miyata.hirokatsu@canon.co.jp

Published online: 15 August 2004; doi:10.1038/nmat1184

Films of mesoporous materials attract broad interest because of their wide applicability in the fields of optics and electronics. Although many of these films have a regular local porous structure, the structural regularity has not been used practically yet because of difficulties in its control on macroscopic scales. Here, we demonstrate the preparation of mesoporous silica films whose porous structure can be described as a single crystal, that is, a long-range order of cage-like pores is maintained over centimetre scales. These films have a three-dimensional hexagonal (space group $P6_3/mmc$) porous structure, and the in-plane arrangement of the pores is strictly controlled by a polymeric substrate surface that has been treated by rubbing. This new class of single-crystalline films with mesoscopic periodic structure is a significant breakthrough in bottom-up nanotechnology, and could lead to novel devices, for example, optics in a soft X-ray region, and quantum electronics.

Since their discovery in the early 1990s[1,2], a great deal of research effort has been directed towards the investigation of mesostructured materials prepared through self-assembly of surfactants. The research area covers the preparation[3–6], characterization[7,8], morphological control[9–12], incorporation of guest species[13–16], and so on. Mesoporous silica films[9,10,17–20] are of special interest because of their application to optical and electronic devices such as lasers[21,22] sensors[23], and photochromic films[24]. Many of the mesoporous silica films have a periodic regular porous structure for which a distinct space group can be defined. However, no substantial application has been proposed for the periodic structure of the films so far, because of difficulties in the control of their structure on macroscopic scales. Several groups reported the alignment control of tubular mesopores in mesoporous silica using the reactant flow[25,26], shearing[27] and strong magnetic field[28]. We reported full alignment control of tubular mesopores in mesoporous silica films using various substrates with surface structural anisotropy[29–32]. Especially, a rubbing-treated polyimide coating gives excellent uniaxial alignment, and the interfacial hydrophobic interaction between the alkyl chain of the surfactant and the elongated polymer chains is considered to direct the surface micelle alignment[31,32].

In this paper, we report the formation of mesoporous silica films with a single-crystalline three-dimensional (3D) hexagonal ($P6_3/mmc$) porous structure. In these films, the in-plane arrangement of the cage-like pores is wholly controlled over centimetre scales (Figure 1). The films are prepared through epitaxial growth of a self-organized mixture of hydrolysed silicon alkoxide and structure-directing agent on the rubbing-treated polyimide coating[31,32]. The structure-directing agent is optimized to provide spherical micelles on the substrate by mixing nonionic surfactants with different head-group sizes. A series of X-ray diffraction (XRD) experiments together with transmission electron microscopy (TEM) established the total porous structure of the films as a vertically shrunk 3D-hexagonal structure ($P6_3/mmc$) with

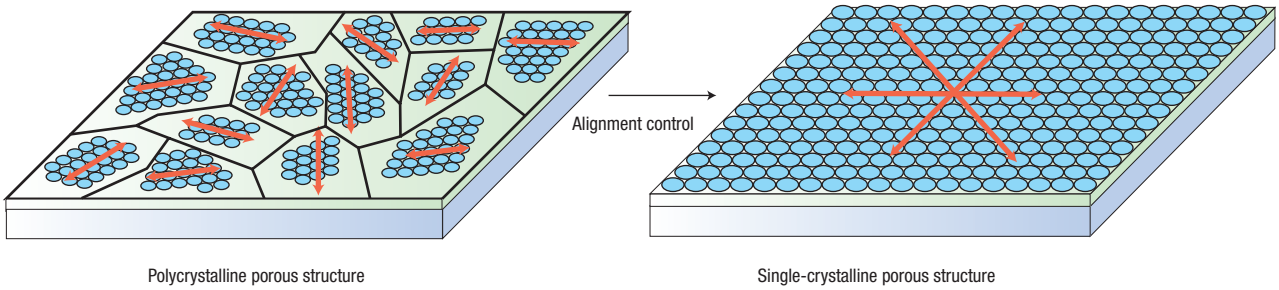

Figure 1 **Illustration showing the single-crystalline porous structure of the present mesoporous silica films in contrast to the conventional films having a polycrystalline porous structure.**

macroscopic in-plane structural regularity. We consider that the formation mechanism of this single-crystalline mesoporous structure includes an initial gradual phase transition of aligned tube-like micelles into spherical ones without losing the in-plane structural regularity. The surface micelle structure thus formed in the early stages of the film formation would work as a scaffold for the subsequent growth of the mesostructured silica film with a 3D-hexagonal structure. The present strategy is, therefore, conceptually different from the previous one in which direct interactions between the surfactant and the anisotropic polymeric surface lead to the formation of mesosporous silica films with uniaxially aligned tubular pores.

Although no atomic-scaled structural ordering is found in the present films, they can be described as artificial single-crystalline films with a mesoscopic periodic structure in contrast to the conventional 'polycrystalline' films in which the in-plane arrangement of the pores is not controlled (Figure 1). These mesoporous films with a single-crystalline porous structure will find many applications in optics and electronics that require the high structural regularity.

The substrate used for the preparation of the present mesoporous silica films is a silica glass substrate coated with polyimide. The polyimide film on the substrate undergoes the rubbing treatment, which is described in detail in previous papers[31,32]. The substrate is kept in the aqueous reactant solution containing surfactants, hydrochloric acid (HCl) and tetraethoxysilane (TEOS) with the molar ratio of surfactant 0.0088/TEOS 0.10/HCl 3/H_2O 100. Mixtures of the two nonionic surfactants, polyoxyethylene 10 cetyl ether ($C_{16}EO_{10}$) and polyoxyethylene 20 cetyl ether ($C_{16}EO_{20}$), were used as structure-directing reagents. The vessel containing the substrate and the reactant solution was sealed at 80 °C for the growth of the mesostructured silica films. The surfactants were removed by calcination under an air atmosphere at 540 °C for 10 h.

The TEM images of the as-grown film prepared using the surfactant mixture of $C_{16}EO_{10}/C_{16}EO_{20}$ = 2:1 are shown in Fig. 2. The image of the cross-section parallel to the rubbing direction and the corresponding electron diffraction (ED) pattern shown in Fig. 2a are consistent with a 3D-hexagonal porous structure consisting of spherical micelles, stacked in the [001] direction. The TEM image and the corresponding ED pattern are different from those shown in Fig. 2b, in which the cross-section is perpendicular to the rubbing direction. These data are also consistent with the above-mentioned 3D-hexagonal structure. Although the detailed TEM observation shows the existence of small stacking faults, the 3D-hexagonal structure is dominant in the film. Figure 2c and d are images reconstructed by extracting the periodic components in the fast Fourier-transformed (FFT) images of Fig. 2a and b, respectively. These images are substantially the same as the corresponding model of the hexagonal structure shown as insets. The actual structure of this film is vertically shrunk, that is, it deviates from the 3D-hexagonal conformation, because shrinkage of the periodic structure occurs selectively in the vertical direction. The deviation from the 3D-hexagonal structure was estimated to be 24.0% for this as-grown film. The TEM image of the film plane is shown in Fig. 2e. Hexagonally aligned pores are observed in the whole area, and the single-crystalline porous structure is confirmed by the higher-order diffraction spots in the corresponding ED pattern. Figure 2f, the reconstructed image of Fig. 2e from its FFT image, clearly shows that the alignment direction of the pores is fixed over the whole of the film.

Although TEM is a powerful tool in determining the structure of mesostructured materials, the images provide only local structural information. Although an electron diffraction pattern provides averaged information, the volume related to the diffraction is still very small. Therefore, we carried out a series of detailed XRD experiments to prove the macroscopic structural regularity.

Figure 3a shows the 2D-XRD patterns of the as-grown film prepared using the surfactant mixture of $C_{16}EO_{10}/C_{16}EO_{20}$ = 2:1, recorded with different sample rotation angles (ϕ). Although the structure deviates from the 3D-hexagonal structure, the Miller indices in the figure are based on a hexagonal structure for easier understanding. The observed strong ϕ dependence of the diffraction pattern clearly shows the single-crystal-like structural feature of this film. Each diffraction pattern was independent of the position in the film as long as the sample rotation angle was fixed. This shows that the film is highly uniform and the in-plane arrangement of the pores is completely controlled over the whole area of the film. The space group of the structure was determined to be $P6_3/mmc$ from these XRD patterns on the basis of the extinction rule. These 2D-XRD patterns are all consistent with the TEM images. The 2D-XRD patterns have no streaks, that is, each diffraction spot is isolated. The extra spots adjoining the main spots are caused by the reflection effect at the substrate surface[33]. These distinct patterns prove that the density of stacking faults is low, which is proven by TEM observation.

The structural anisotropy of this film can be quantified by in-plane XRD. This geometry, shown as the inset of Fig. 3b, enables the analysis of the upright lattice planes, and has been used to evaluate the in-plane alignment of the tubular mesopores in 2D-hexagonal mesostructured silica films[29–32].

Figure 3b shows the ϕ–$2\theta\chi$ scanning profiles of this film. Traces A and B were recorded with the sample geometries in which the rubbing direction was set perpendicular and parallel to the X-rays at ϕ = 0°, respectively. In trace A, two distinct diffraction peaks were observed at $2\theta\chi$ = 1.18° and 2.36°. On the other hand, in trace B, the intensity of these peaks was remarkably decreased, and a new weak peak was observed at $2\theta\chi$ = 2.05°. The difference between these in-plane XRD profiles results from the strong in-plane structural anisotropy of this film.

The ϕ scanning profile of the film fixing the detector at a position of $2\theta\chi$ = 1.18° is shown as trace A in Fig. 3c. Six sharp diffraction peaks are

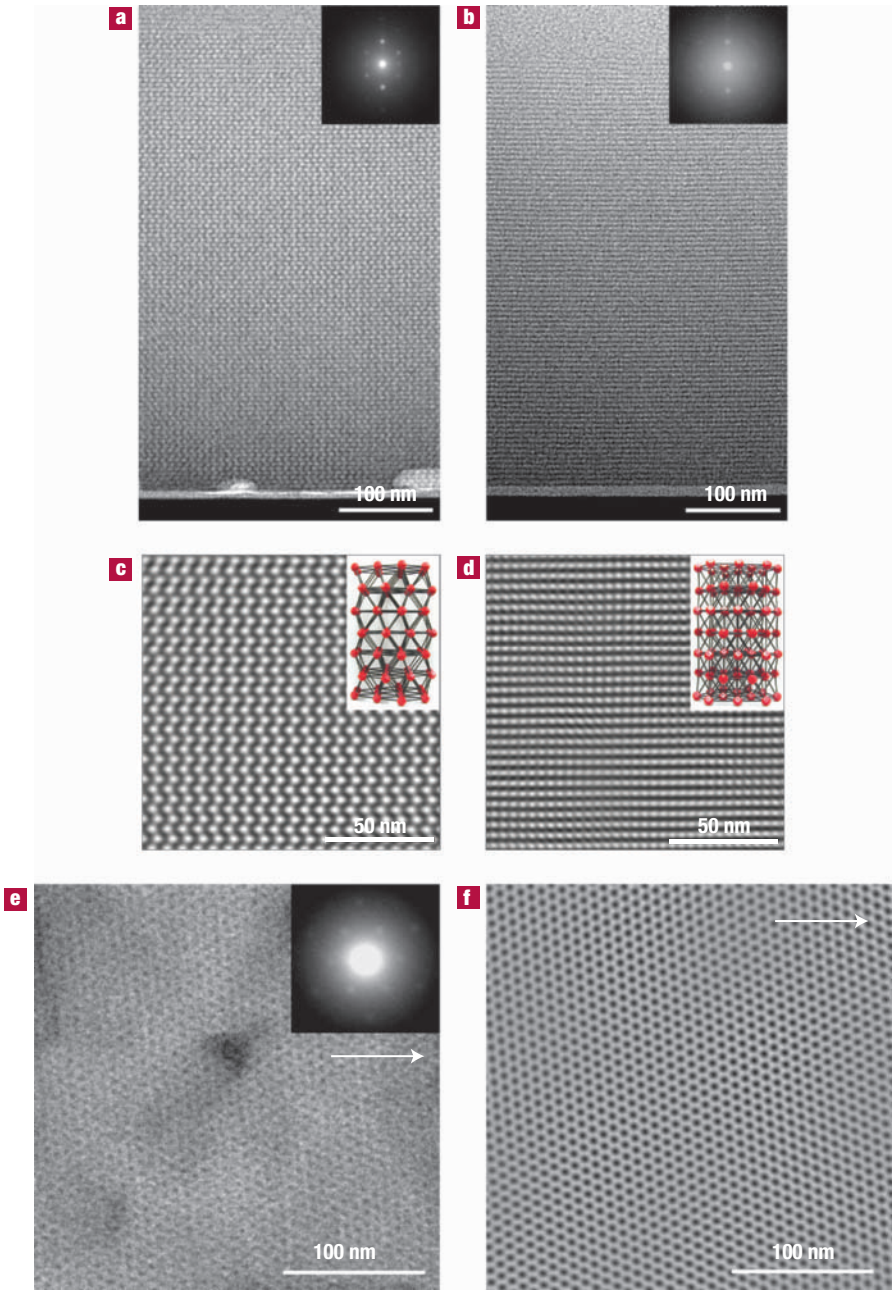

Figure 2 TEM images of the as-grown film with a single-crystalline porous structure prepared using the surfactant mixture of $C_{16}EO_{10}/C_{16}EO_{20} = 2:1$. a,**b**, Cross-sectional image of the film sliced parallel (**a**) and perpendicular (**b**) to the rubbing direction. Insets: corresponding ED patterns. **c**,**d**, Reconstructed cross-sectional images parallel (**c**) and perpendicular (**d**) to the rubbing direction obtained by extracting the periodic components from the FFT images of **a** and **b**. Insets: corresponding models of 3D-hexagonal ($P6_3/mmc$) structure. **e**, Top-view image of the film. Inset: corresponding ED pattern. The irregular contrast is caused by the uneven surface of the epoxy resin used for the protection of the thin specimen. **f**, Reconstructed image from the FFT image of **e**. The arrows in **e** and **f** show the rubbing direction.

observed with an interval of 60.0°, showing that the in-plane arrangement of the spherical micelles is strictly controlled over the whole film. The peak intensity was minimum when the rubbing direction was parallel to the X-ray incidence ($\phi = 0°$), and the intensity maxima were observed at $\phi = \pm 30°$, $\pm 90°$ and $\pm 150°$. From these data, together with the above 2D-XRD patterns, the observed peak at $2\theta\chi = 1.18°$ and 2.36° can be assigned to $(1\bar{1}l)$ and $(2\bar{2}l)$, respectively. The in-plane rocking curve was recorded also for the diffraction peak at $2\theta\chi = 2.05°$ (trace B in Fig. 3b). Six sharp diffraction peaks were observed in the rocking curve also in this case, but the positions of the peaks were shifted by 30°, as shown in trace B in Fig. 3c. From this result, the diffraction peak at $2\theta\chi = 2.05°$ is assigned to $(1\bar{2}0)$. The observed XRD data are all consistent with both the proposed vertically shrunk 3D-hexagonal ($P6_3/mmc$) structure and the TEM images.

In general, this kind of well-resolved rocking curve is obtained only when the film has a single-crystalline structure. Although no

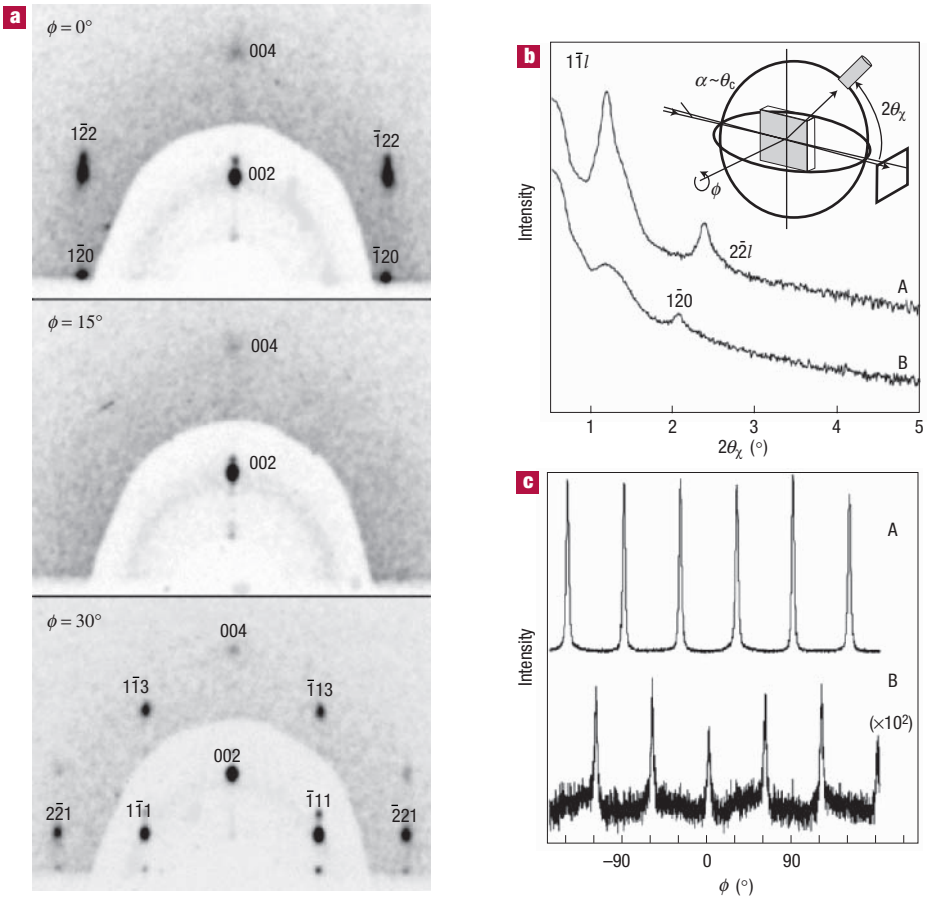

Figure 3 XRD patterns of the as-grown single-crystalline film prepared using the surfactant mixture of $C_{16}EO_{10}/C_{16}EO_{20}$ = 2:1. a, 2D-XRD patterns recorded for the different sample rotation angles. **b**, ϕ–$2\theta\chi$ scanning profiles recorded when the projection of the incident X-rays is perpendicular (A) and parallel (B) to the rubbing direction at $\phi = 0°$. Inset: scanning axes of the in-plane XRD geometry. The index of ($1\bar{1}l$) represents ($1\bar{1}1$) and ($1\bar{1}0$), and ($2\bar{2}l$) represents ($2\bar{2}1$) and ($2\bar{2}0$). ($1\bar{1}1$) and ($2\bar{2}1$) predominantly contribute to the each diffraction peak. **c**, ϕ scanning profiles at $2\theta\chi = 1.18°$ (A), and $2\theta\chi = 2.05°$ (B).

atomic-scaled structural regularity is observed in the silica pore walls, the mesoscaled structural regularity causes various features that are observed for crystalline materials, such as crystal-like particle morphologies[8,34] and existence of sharp X-ray diffraction peaks. It is appropriate to regard these films as 'single-crystalline' with a structural period more than ten times larger than that of real crystals consisting of atoms. The mesoporous silica films with a 3D porous structure reported so far are all 'polycrystalline' films, in which no macroscopic preferential orientation is observed for the porous structure in the plane of the film[35].

In the present mesostructured silica film, because the underlying polyimide is thin enough (~10 nm), the surfactants in the pores can be removed by calcination without peeling of the film from the substrate. The in-plane structural regularity is completely retained after surfactant removal. The profiles of the in-plane XRD patterns are substantially unchanged by calcination (see Supplementary Information, Fig. S1). Thus, the formation of single-crystalline 3D-hexagonal mesoporous silica films was confirmed. However, the structural period in the vertical direction shrunk by 20.0% through calcination (data not shown) because of the condensation of the silanol groups, and consequently, the deviation from the 3D-hexagonal structure increased from 24.0% to 39.4%.

The in-plane structural regularity strongly depends on the mixing ratio of $C_{16}EO_{10}$ and $C_{16}EO_{20}$. Figure 4a shows the ϕ scanning profiles of ($1\bar{1}l$) recorded for the films prepared using the surfactant mixture at different mixing ratios. The width of the diffraction peaks, depending on the degree of the in-plane structural fluctuation, became narrower with increasing $C_{16}EO_{10}/C_{16}EO_{20}$ ratio. In these films, the total molar ratio of the surfactant to other components was fixed. It is worth noting that the mesoporous silica film with a single-crystalline porous structure cannot be formed with only one component of the surfactant mixture under the present conditions. These facts suggest that the addition of $C_{16}EO_{10}$ largely affects the micelle structure on the rubbing-treated polyimide surface. The mixing ratio does not affect the size of the micelles because the structural periods estimated from ϕ–$2\theta\chi$ scanning profiles are independent of the mixing ratio (data not shown). However, the addition of $C_{16}EO_{10}$ can affect the shape of the micelles. For the heterogeneous reaction involved in the present mesostructured silica film growth, the concentration and the molar ratio of the two surfactants at the substrate surface can be different from those in the solution, depending on the respective distribution coefficient. Therefore, the local concentration of one of the two surfactants at the surface can be selectively higher. In the present system, the local concentration of $C_{16}EO_{10}$ on the surface would be higher than that of $C_{16}EO_{20}$ because of the smaller hydrophilic group. This might lead to the formation of an aligned tube-like surface micelle structure in the early stages of the film formation, similar to that

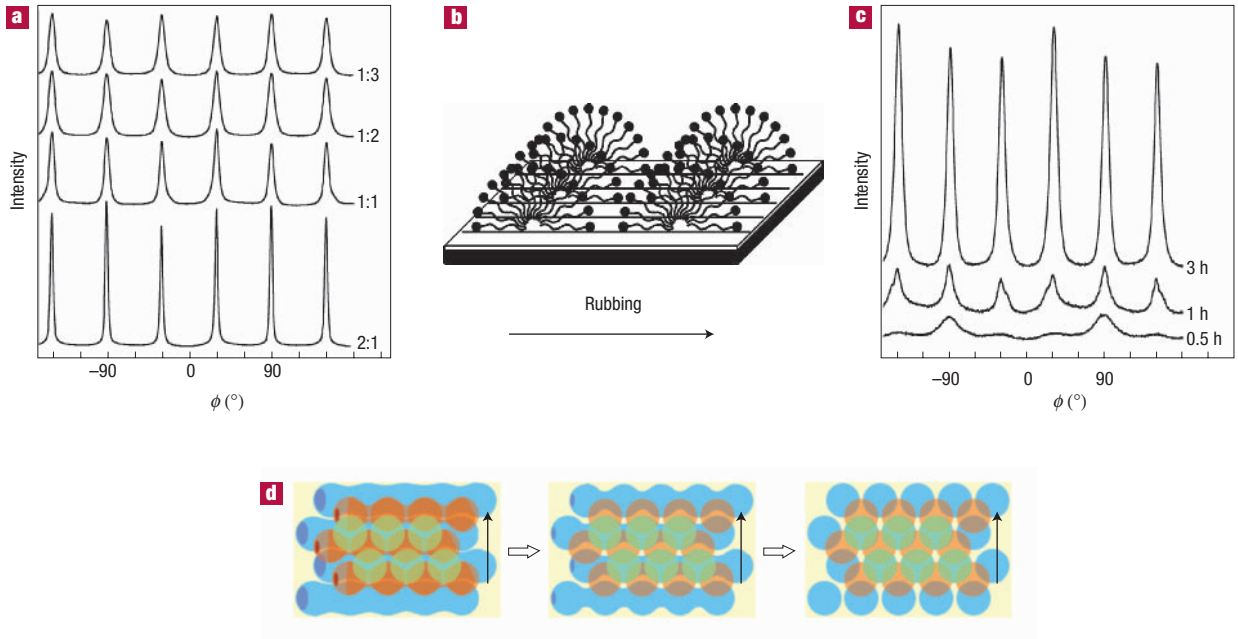

Figure 4 Variation of the porous structure with the surfactant mixing ratio and the reaction time, and the proposed mechanism for the in-plane regular stacking of the spherical micelles. a, ϕ scanning XRD profiles of the as-grown films prepared using the surfactant mixtures with different molar ratios; $C_{16}EO_{10}/C_{16}EO_{20}$ = 1:3, 1:2, 1/:1 and 2:1. **b**, Alignment model of the tubular pores on the rubbing-treated polyimide. **c**, ϕ scanning XRD profiles in the early stages of the film formation prepared using the surfactant mixture of $C_{16}EO_{10}/C_{16}EO_{20}$ = 2:1. **d**, Illustration of the formation mechanism of the mesostructured silica film with a single-crystalline porous structure. The rubbing direction is shown as vertical arrows in the figure. First, the aligned tubular micelles are formed on the substrate perpendicular to the rubbing direction, and the tubular micelles are transformed into spherical ones in the early stages of the film formation. The first layer (blue), for which the interactions with the substrate are strongest, is also transformed. The surface micelle structure acts as a scaffold for the growth of the mesostructured silica film with the 3D-hexagonal structure.

formed when $C_{16}EO_{10}$ was used alone[32]. In this case, tubular mesochannels are aligned perpendicularly to the rubbing direction through interfacial hydrophobic interactions as schematically shown in Fig. 4b. This aligned tube-like surface micelle structure can cause the observed in-plane structural regularity of the 3D-hexagonal phase.

To prove this mechanism, the early stages of the film formation were investigated. Figure 4c shows the ϕ scanning profiles of the main in-plane XRD peaks recorded for the films prepared using the surfactant mixture of $C_{16}EO_{10}/C_{16}EO_{20}$ = 2:1, with different times for the film growth. The sample films on the substrates were taken from the reactant solution after 30 min, 1 h and 3 h contact with the reactant solution. For the film grown for 30 min, only two weak peaks were observed in the ϕ scanning profile. This shows that the tube-like micelles wrapped with silica are aligned perpendicularly to the rubbing direction in this stage. Though the diffraction intensity is weak, the distinct two XRD peaks in the ϕ scanning profile indicate the formation of a multilayered mesostructured silica film with an aligned 2D-hexagonal structure. The broad peaks suggest the relatively poor alignment of the micelles. Even though the relative concentration of $C_{16}EO_{10}$ on the substrate surface is higher than in the solution, $C_{16}EO_{20}$—preferring a higher curvature of the micelles—can disturb the regularity of the surface micelle structure. After the film growth for 1 h, six broad diffraction peaks were observed in the ϕ scanning profile, indicating that phase transition from the tubular micelles into the 3D-hexagonal structure took place between 30 min and 1 h. In the early stages of the film formation, condensation of silanol groups in the pore walls decreases the density of the active sites that interact with the head groups of the nonionic surfactants. This would prompt the transformation of the tubular micelles to spherical ones with higher curvature, which is favoured by $C_{16}EO_{20}$. The whole of the initial multilayered film with the aligned 2D-hexagonal structure would gradually be transformed into the 3D-hexagonal structure, leading to the formation of the mesostructured silica films with the single-crystalline porous structure. The phase transition may take place unevenly along the film thickness because the first layer on the substrate should be strongly restricted by the surface. The 3D-hexagonal film thus formed through phase transition may act as a scaffold for the subsequent epitaxial growth of the spherical silica–micelle building blocks for the formation of the thicker films. The formation mechanism of the present films is schematically shown in Fig. 4d. The proposed model is supported by the TEM images that clearly prove the existence of the spherical micelles in the first layer on the substrate.

Present electronics and optics are based on an atomic-scaled structural period of crystals, and submicrometre-scaled periodic structure can be applied to photonic crystals. The mesoporous films with a single-crystalline porous structure over centimetre scales have potential to be applied in various new fields; for example, in optical devices in a soft (low energy) X-ray region because the structural period of the films is comparable to the wavelength. Again, these films may be used as templates for the preparation of regular 3D array of nanocrystals, which can be applied to devices of quantum electronics.

METHODS

The TEM images were recorded on a Hitachi H-800 at an accelerating voltage of 200 kV. The specimen for the cross-sectional TEM observation was prepared as follows; first, the sample was embedded in an epoxy

resin and a piece with a thickness of ~500 μm was sawed off; second, the piece was mechanically pre-thinned and polished by a disk grinder and a dimple grinder to produce a central region of ~10 μm thick; and finally, the central region was milled with two Ar^+ ion beams of 3 keV energy with incident angles –1° and 4°, respectively.

The 2D-XRD patterns were recorded under a reflection geometry using synchrotron radiation at the Photon Factory (KEK Japan) on beam-line 4A. A 3 μm × 3μm X-ray microbeam with 8 keV was used, and the diffraction patterns were recorded using an X-ray charge-coupled device detector with image intensifier. The in-plane XRD patterns were recorded with an X-ray diffractometer equipped with a four-axes goniometer (Rigaku ATX-G) using CuKα radiation. The incident angle of X-rays in the in-plane geometry was set to 0.2°. Because of the small incident angle, the whole of the film contributes to the observed diffraction.

Received 13 April 2004; accepted 17 June 2004; published 15 August 2004.

References

1. Yanagisawa, T., Shimizu, T., Kuroda, K. & Kato, C. The preparation of alkyltrimethylammonium-kanemite complexes and their conversion to microporous materials. *Bull. Chem. Soc. Jpn* **63,** 988–992 (1990).
2. Kresge, C. T., Leonowicz, M. E., Roth, W. J., Vartuli, J. C. & Beck, J. S. Ordered mesoporous molecular sieves synthesized by a liquid-crystal template mechanism. *Nature* **359,** 710–712 (1992).
3. Huo, Q. *et al.* Generalized synthesis of periodic surfactant/inorganic composite materials. *Nature* **368,** 317–321 (1994).
4. Zhao, D. *et al.* Triblock copolymer synthesis of mesoporous silica with periodic 50 to 300 ångstrom pores. *Science* **279,** 548–552 (1998).
5. Yang, P., Zhao, D., Margolese, D. I., Chmelka, B. F. & Stucky, G. D. Generalized syntheses of large-pore mesoporous metal oxides with semicrystalline frameworks. *Nature* **396,** 152–155 (1998).
6. Attard, G. S., Glyde, J. C. & Göltner, C. G. Liquid-crystalline phases as templates for the synthesis of mesoporous silica. *Nature* **378,** 366–368 (1995).
7. Firouzi, A. *et al.* Cooperative organization of inorganic-surfactant and biomimetic assemblies. *Science* **267,** 1138–1143 (1995).
8. Sakamoto, Y. *et al.* Direct imaging of the pores and cages of three-dimensional mesoporous materials. *Nature* **408,** 449–453 (2000).
9. Yang, H., Kuperman, A., Coombs, N., Mamiche-Afara, S. & Ozin, G. A. Synthesis of oriented films of mesoporous silica on mica. *Nature* **379,** 703–705 (1996).
10. Lu, Y. *et al.* Continuous formation of supported cubic and hexagonal mesoporous films by sol-gel dip-coating. *Nature* **389,** 364–368 (1997).
11. Schacht, S., Huo, Q., Voigt-Martin, I. G., Stucky, G. D. & Schüth, F. Oil-water interface templating of mesoporous macroscale structures. *Science* **273,** 768–771 (1996).
12. Huo, Q. *et al.* Room temperature growth of mesoporous silica fibers: a new high-surface-area optical waveguide. *Adv. Mater.* **9,** 974–978 (1997).
13. Nguyen, T.-Q., Wu, J., Doan, V., Schwartz, B. J. & Tolbert, S. H. Control of energy transfer in oriented conjugated polymer-mesoporous silica composites. *Science* **288,** 652–656 (2000).
14. Takahashi, H. *et al.* Catalytic activity in organic solvents and stability of immobilized enzymes depend on the pore size and surface characteristics of mesoporous silica. *Chem. Mater.* **12,** 3301–3305 (2000).
15. Mal, N. K., Fujiwara, M. & Tanaka, Y. Photocontrolled reversible release of guest molecules from coumarin-modified mesoporous silica. *Nature* **421,** 350–353 (2003).
16. Dag. Ö., Ozin, G. A., Yang, H., Reber, C. & Bussière, G. Photoluminescent silicon clusters in oriented hexagonal mesoporous silica film. *Adv. Mater.* **11,** 474–480 (1999).
17. Yang, H., Coombs, N., Sokolov, I. & Ozin, G. A. Free-standing and oriented mesoporous silica films grown at the air-water interface. *Nature* **381,** 589–592 (1996).
18. Ogawa, M. Formation of novel oriented transparent films of layered silica-surfactant nanocomposites. *J. Am. Chem. Soc.* **116,** 7941–7942 (1994).
19. Aksay, I. A. *et al.* Biomimetic pathways for assembling inorganic thin films. *Science* **273,** 892–897 (1996).
20. Tolbert, S. H., Schäffer, T. E., Feng, J., Hansma, P. K. & Stucky, G. D. A new phase of oriented mesoporous silicate thin films. *Chem. Mater.* **9,** 1962–1967 (1997).
21. Marlow, F., McGehee, M. D., Zhao, D., Chmelka, B. F. & Stucky, G. D. Doped mesoporous silica fibers: a new laser material. *Adv. Mater.* **11,** 632–636 (1999).
22. Yang, P. *et al.* Mirrorless lasing from mesostructured waveguides patterned by soft lithography. *Science* **287,** 465–467 (2000).
23. Wirnsberger, G., Scott, B. J. & Stucky, G. D. pH sensing with mesoporous thin films. *Chem. Commun.*, 119–120 (2001).
24. Wirnsberger, G., Scott, B. J., Chmelka, B. F. & Stucky, G. D. Fast response photochromic mesostructures. *Adv. Mater.* **12,** 1450–1454 (2000).
25. Trau, M. *et al.* Microscopic patterning of oriented mesoscopic silica through guided growth. *Nature* **390,** 674–676 (1997).
26. Hillhouse, H. W., Okubo, T., van Egmond, J. W. & Tsapatsis, M. Preparation of supported mesoporous silica layers in a continuous flow cell. *Chem. Mater.* **9,** 1505–1507 (1997).
27. Melosh, N. A., Davidson, P., Feng, P., Pine, D. J. & Chmelka, B. F. Macroscopic shear alignment of bulk transparent mesostructured silica. *J. Am. Chem. Soc.* **123,** 1240–1241 (2001).
28. Tolbert, S. H., Firouzi, A., Stucky, G. D. & Chmelka, B. F. Magnetic field alignment of ordered silicate-surfactant composites and mesoporous silica. *Science* **278,** 264–268 (1997).
29. Miyata, H. & Kuroda, K. Preferred alignment of mesochannels in a mesoporous silica film grown on a silicon (110) surface. *J. Am. Chem. Soc.* **121,**7618–7624 (1999).
30. Miyata, H. & Kuroda, K. Alignment of mesostructured silica on a Langmuir-Blodgett Film. *Adv. Mater.* **11,** 1448–1452 (1999).
31. Miyata, H. & Kuroda, K. Formation of a continuous mesoporous silica film with fully aligned mesochannels on a glass substrate. *Chem. Mater.* **12,** 49–54 (2000).
32. Miyata, H., Noma, T., Watanabe, M. & Kuroda, K. Preparation of mesoporous silica films with fully aligned large mesochannels using nonionic surfactants. *Chem. Mater.* **14,** 766–772 (2002).
33. Noma, T., Takada, K., Miyata, H. & Iida, I. X-ray micro diffraction study on mesostructured silica thin films. *Nucl. Inst. Meth. A* **467–468,** 1021–1025 (2001).
34. Guan, S., Inagaki, S., Ohsuna, T. & Terasaki, O. Cubic hybrid organic-inorganic mesoporous crystal with a decaoctahedral shape. *J. Am. Chem. Soc.* **122,** 5660–5661 (2000).
35. Soler-Illia, G. J. A. A., Crepaldi, E. L., Grosso, D., Durand, D. & Sanchez, C. Structural control in self-standing mesostructured silica oriented membranes and xerogels. *Chem. Commun.* 2298–2299 (2002).

Acknowledgements

The authors acknowledge O. Terasaki for useful discussions about the TEM images, and Y. Sugahra, T. Yonehara and O. Albrecht for helpful comments. The work was partially supported by Grant-in-Aids for COE research (Molecular nanoengineering) and 21COE program (Practical nanochemistry), MEXT, Japan.

Correspondence and requests for materials should be addressed to H.M.

Supplementary Information accompanies the paper on www.nature.com/naturematerials

Competing financial interests

The authors declare that they have no competing financial interests.